Diffusion Foundations
ISSN: 2296-3642, Vol. 27, pp 90-98
doi:10.4028/www.scientific.net/DF.27.90

Submitted: 2019-09-11
Accepted: 2019-12-01
Online: 2020-05-05

Microstructure and Properties of Lead-Free Perovskite Ceramics on the Base of KNN Perovskite

E.D. Politova[1], G.M. Kaleva[1], A.V. Mosunov[1], N.V. Sadovskaya[1], D.A. Kiselev[2,3], A.M. Kislyuk[2], T.S. Ilina[2], S. Yu. Stefanovich[1,4]

[1]L.Ya.Karpov Institute of Physical Chemistry; Vorontsovo pole, 10, Moscow 105064 Russia,

[2]National University of Science and Technology "MISiS", Leninskii pr. 4, Moscow, 119049 Russia,

[3]Fryazino branch of the Kotel'nikov Institute of Radioengineering and Electronics of Russian Academy of Sciences, Vvedensky Square 1, Fryazino, Moscow region, 141190 Russia,

[4]Lomonosov Moscow State University, Leninskie gory 1, Moscow 119992 Russia,

E-mail: politova@nifhi.ru

Keywords: sodium-potassium niobate, perovskite structure, microstructure, properties

Abstract. The influence of $LiSbO_3$ on the structure, microstructure, dielectric, ferroelectric and local piezoelectric properties of $(K_{0.5}Na_{0.5})NbO_3$ ceramics has been studied. Changes in unit cell parameters correlated with ionic radii changes and high effective local d_{33} piezoelectric coefficient values were observed depending on solid solutions compositions.

Introduction

Based on potassium-sodium niobate $(K,Na)NbO_3$ (KNN) perovskite ceramics continue to be among the most intensively studied in the last decade because they are among the most promising materials for the toxic lead oxide containing materials replacement [1 - 21]. In the $KNbO_3 – NaNbO_3$ system a composition (50/50) comprises a complete solid solution of antiferroelectric $NaNbO_3$ and ferroelectric $KNbO_3$ [7]. This composition is close to the MPB between two orthorhombic phases and is characterized by two composition-independent phase transitions with temperatures between ferroelectric phases near 470 K and between ferroelectric and paraelectric phases at 670 K [22].

Piezoelectric properties of materials based on KNN are determined by the ratio of orthorhombic (O) and tetragonal (T) phases, so in order to improve piezoelectric response changes in KNN-based compositions are necessary in order to shift the transition temperature from orthorhombic to tetragonal phase to room temperature [8, 9, 12, 15]. Difficulties in preparation of stoichiometric compositions due to the presence of high volatile potassium and sodium oxides and because of the narrow sintering temperature interval for KNN-based ceramics comprise particular problems [12 - 21]. Besides, the formation of oxygen vacancies in nonstoichiometric compounds leads to the formation of additional dipoles relaxing in an alternating field and leading to an increase in ionic conductivity of the samples [23].

In this work, the effects of modification of KNN compositions by perovskite $LiSbO_3$ with Li^+ dopants in the A-sites and Sb^{5+} substitutions in the B-sites of perovskite lattice on structure, microstructure, dielectric, ferroelectric and local piezoelectric properties of ceramics have been studied. In order to improve the sintering of ceramics the samples were additionally modified by small amounts of overstoichiometric LiF additives [24].

Experimental

Ceramic samples $(1-x)(K_{0.5}Na_{0.5})NbO_3 – xLiSbO_3$ (x=0 - 0.1, with Δx=0.02) were prepared by the solid state reaction method at calcinations temperatures of T_1=973 - 1073 K (6 h), and sintering temperatures of T_2=1273 - 1323 K (2 h). 5 w. % of LiF additives The samples were additionally modified by small amounts of LiF additives in order to improve the sintering of ceramics [24].

Sodium carbonate Na_2CO_3, potassium carbonate K_2CO_3, lithium carbonate Li_2CO_3, Nb_2O_5, and Sb_2O_5 oxides ("pure" grade), and LiF were used as starting materials. Carbonates were dried at 673 K before synthesis in order to remove absorbed water.

Phase content and structure parameters of the samples were characterized by the X-ray Diffraction method (DRON-3M, Cu-K_α radiation with wavelength λ=1.5405 A, in the 2 theta range of 5 – 80 degrees). The Second Harmonic Generation (SHG) method was used to study spontaneous polarization and phase transitions of the samples (Nd:YAG laser, λ=1.064 μm in the reflection). Dielectric measurements were performed with fired silver electrodes on heating with 10 K/min. and cooling in the temperature interval of 300 – 1000 K, in the frequency range of 100 Hz – 1 MHz using Agilent 4284 A (1 V). Microstructure of the samples was examined by the Scanning Electron Microscopy (SEM) method (JEOL YSM-7401F with a JEOL JED-2300 energy dispersive X-ray spectrometer system).

The surface morphology, as-grown domain structure and local piezoelectric hysteresis loops of the samples were characterized by the piezoresponse force microscopy (PFM) method using a commercial scanning probe microscope MFP-3D (Asylum Research, USA) with Ti/Ir coated conductive probes (Asyelec-02, Asylum Research, USA). Before scanning and local switching, the inverse optical lever sensitivity (Δ, nm/V) and spring constant (k, N/m) were calibrated using the GetReal™ Automated Probe Calibration (Asylum Research, USA). An AC voltage (3 V_{pp}) was superimposed onto a triangular square-stepping wave (f = 0.5 Hz, with writing and reading times 25 ms, and bias window up to ±30 V) during the remnant piezoelectric hysteresis loops measurements. For PFM characterization, the samples were polished using polycrystalline diamond with different sizes up to the root mean square roughness of all the samples reached less than 10 nm. Effective piezoelectric coefficient (d_{33} in pm/V) was calculated from PFM phase and PFM amplitude hysteresis loops using Igor Pro software version 6.37 (Asylum Research, USA). In this study, all measurements were repeated at least 4 times in the different locations of the same sample with strong PFM domains contrast.

Results and Discussion

Pure samples with perovskite structure were prepared (Figure 1). However, small amounts of admixture phase $K_2Nb_8O_{21}$ were observed in the X-ray diffraction patterns of the samples with x=0.1.

Initial KNN samples have typical orthorhombic structure. In samples with x≥0.06 coexistence of the orthorhombic and tetragonal phases was revealed at the room temperature (Figures 2, 3) [25]. These results are consistent with the results published earlier [26]. Slight shift of the X-Ray diffraction peaks to higher angles points to a decrease in the unit cell parameters due to introduction of smaller Li^+ and Sb^{5+} cations into A and B-site positions of perovskite lattice, correspondingly. So, the observed changes in the unit cell volume of the KNN-based ceramics correlated well with cation substitutions.

Microstructure of the samples is sensitive to both substitutions and sintering conditions as well (Figure 4). With increasing sintering temperature enlargement of mean size of grains was observed, though mean size of grains decreased with x increasing.

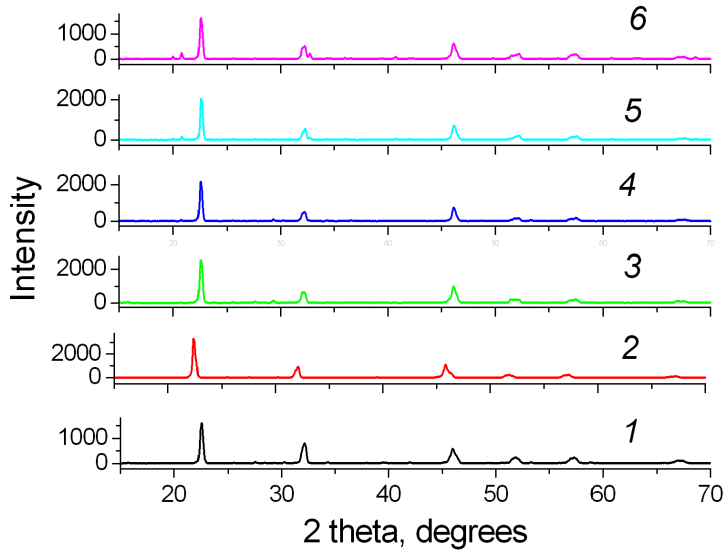

Figure 1 - X-Ray diffraction patterns of the samples (1-x)($K_{0.5}Na_{0.5}$)NbO_3 – $x$$LiSbO_3$ with x=0.0 (*1*), 0.02 (*2*), 0.04 (*3*), 0.06 (*4*), 0.08 (*5*), 0.10 (*6*) doped with LiF.

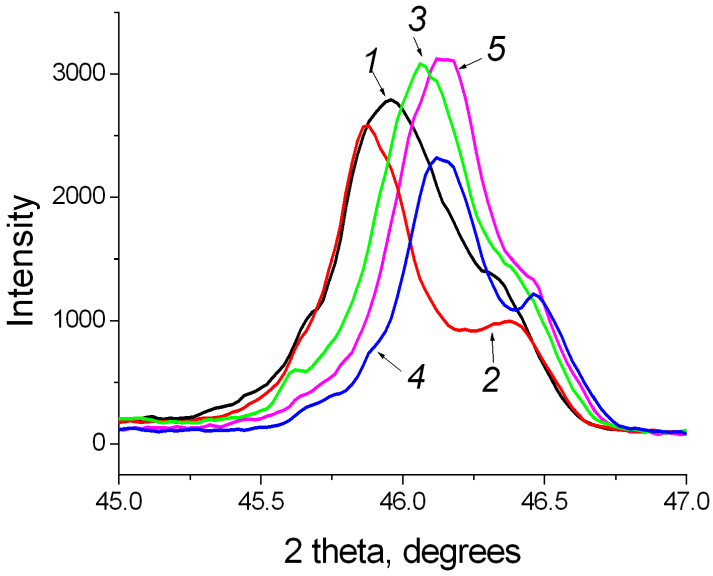

Figure 2 – Parts of the X-Ray diffraction patterns of the LiF doped samples (1-x)($K_{0.5}Na_{0.5}$)NbO_3 – $x$$LiSbO_3$ with x=0.0 (*1*), 0.02 (*2*), 0.04 (*3*), 0.06 (*4*), 0.10 (*5*).

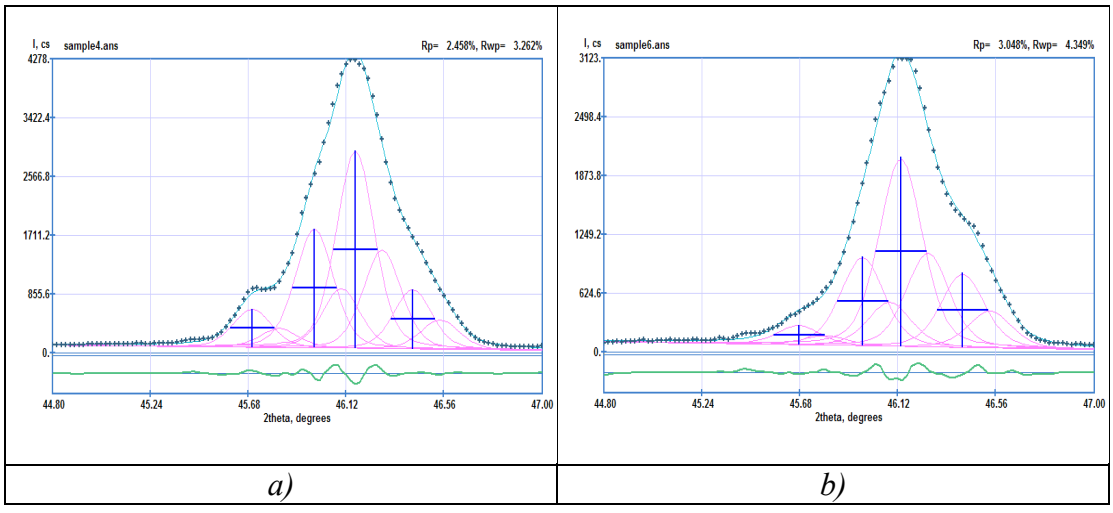

Figure 3 – Simulation of the X-Ray diffraction peaks of the LiF doped samples (1-x)($K_{0.5}Na_{0.5}$)NbO_3 – $x$$LiSbO_3$ with x=0.04 (*a*) and 0.10 (*b*).

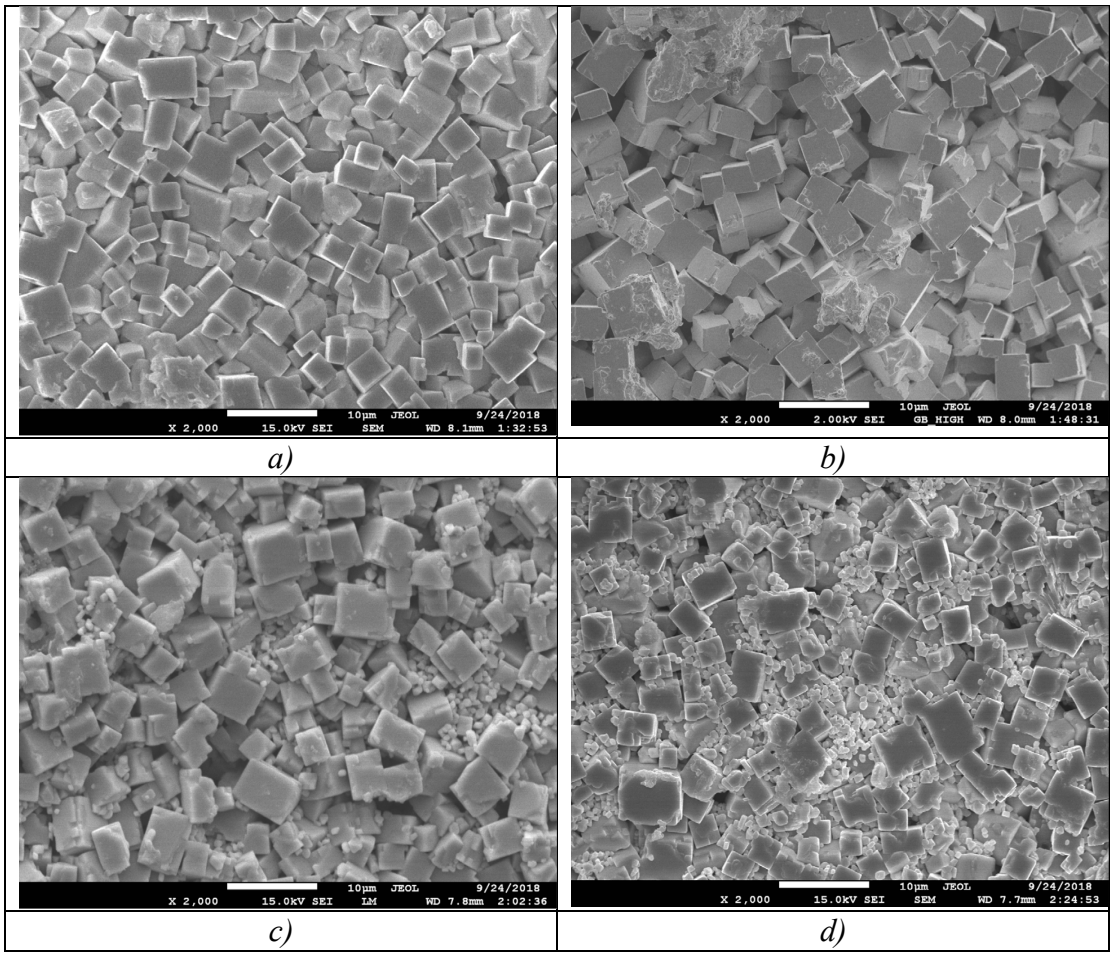

Figure 4 - Microstructure of the samples with x=0 (*a*), 0.04 (*b*), 0.08 (*c*), 0.10 (*d*). Bars – 10 μm.

The SHG method measurements confirmed the polar nature of the samples indicating to their ferroelectric properties (Figure 5*a*). Ferroelectric phase transitions marked by steps were revealed by the SHG method. With increasing $LiSbO_3$ content, increase in intensity of the SHG signal was observed that pointed to an increase in spontaneous polarization of the doped samples (Figure 5*b*).

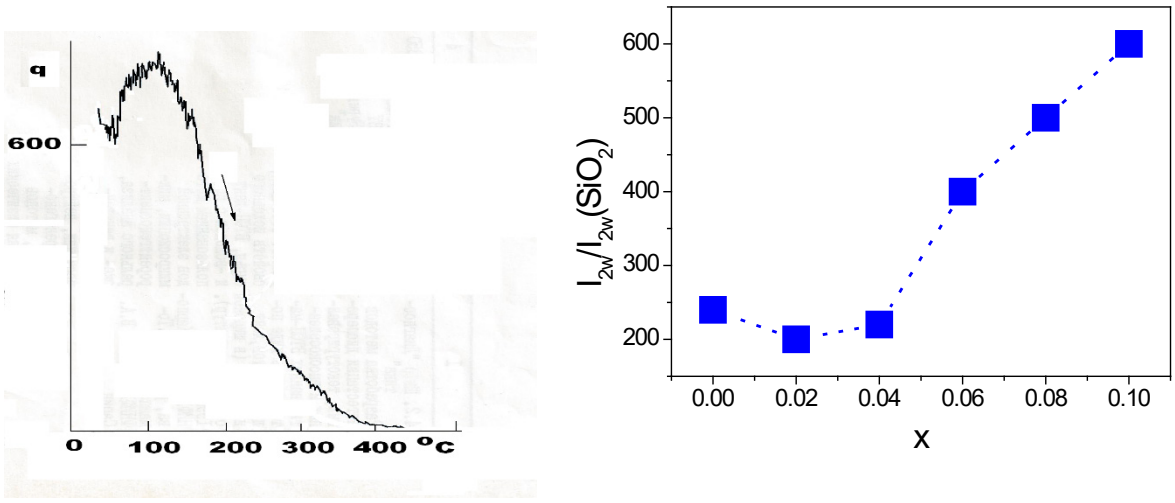

Figure 5 - Temperature dependence of the SHG signal q for the sample with x=0.10 (*a*); concentration dependence of the SHG signal for samples $(1\text{-}x)(K_{0.5}Na_{0.5})NbO_3 - xLiSbO_3$ (*b*).

Accordingly, typical of the KNN-based compositions steps near ~ 350 - 400 K and maxima at ~ 600 – 700 K were revealed in the dielectric permittivity versus temperature curves (Figure 6). Slight decrease in temperature of the phase transition to paraelectric phase T_C, while a great shift of the ferroelectric tetragonal to orthorhombic phase transition to the room temperature were observed in the ceramic samples studied.

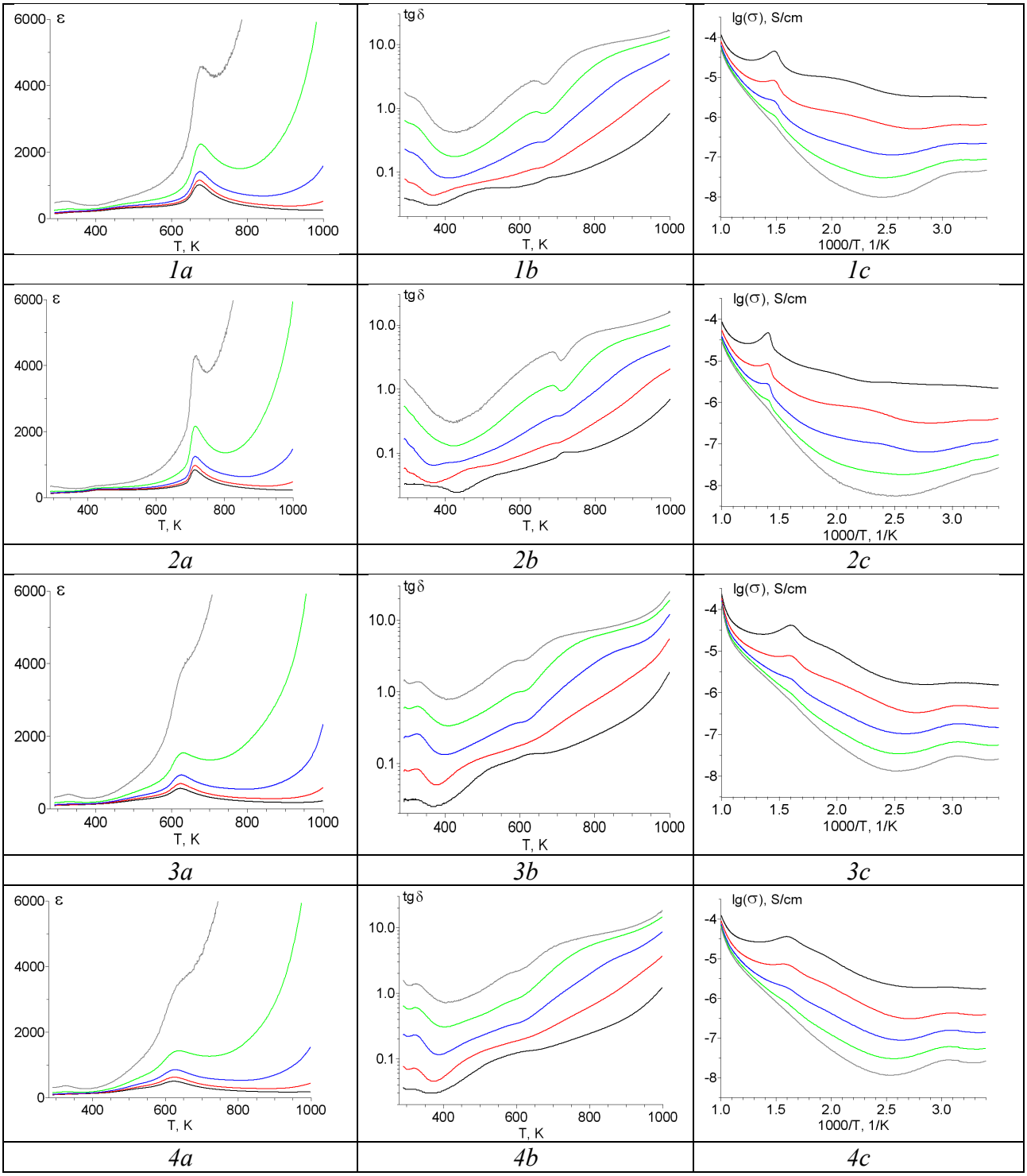

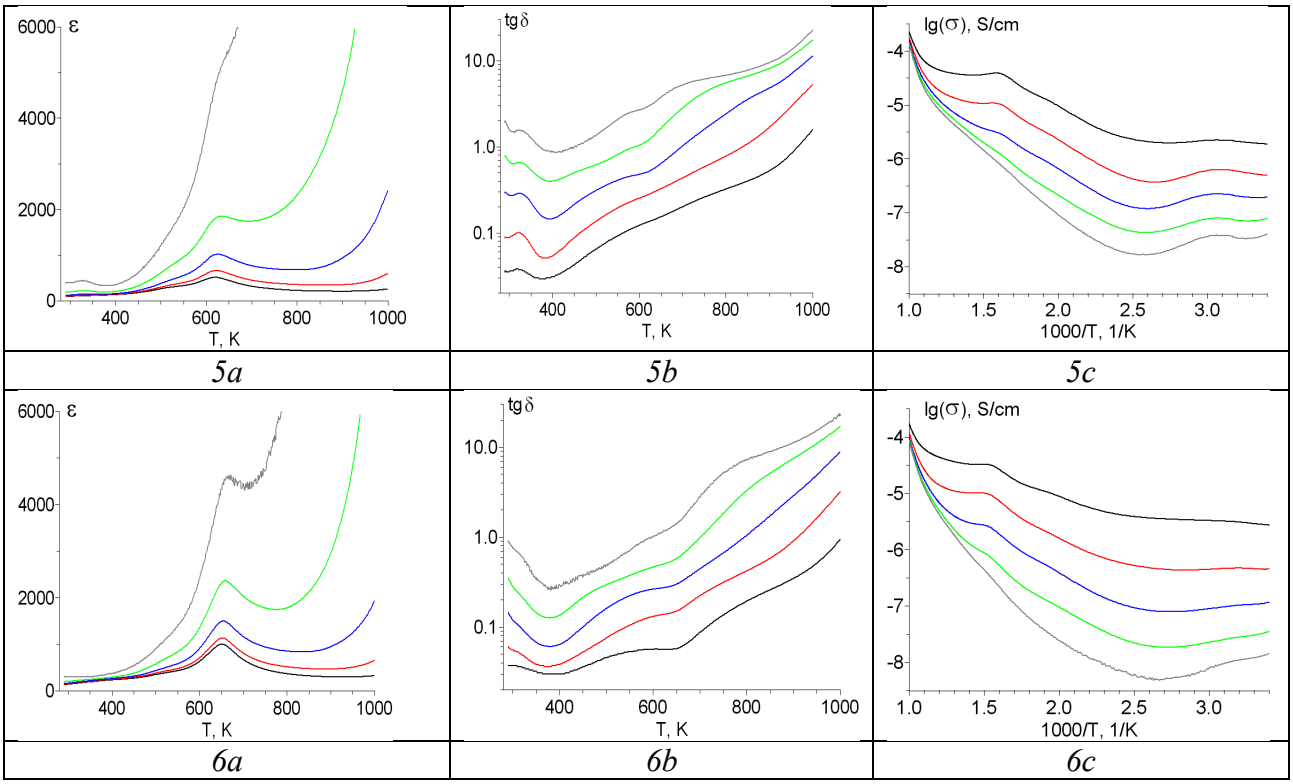

Figure 6 - Temperature dependences of dielectric permittivity $\varepsilon(T)$*(a)*, dielectric loss $\tan\delta(T)$*(b)* and $\lg\sigma(1000/T)$*(c)* of the samples with x=0.0 (*1a-c*), 0.02 (*2a-c*), 0.04 (*3a-c*), 0.06 (*4a-c*), 0,08 (*5a-c*), 0.10 (*6a-c*) sintered at T_2=1403 K (2 h) measured at frequencies f=100 Hz, 1, 10, 100 kHz, 1 MHz.

Using the piezoresponse force microscopy (PFM) method, surface morphology, domain structures and local piezoelectric hysteresis loops of the samples were studied (Figures 7 and 8). Nucleation of single domains occurs under a sharp tip during the PFM testing reflecting development of domains and indicating ferroelectric polarization switching on nanoscale. Simultaneous topography and out-of-plane PFM images showed that the imaged pattern were due to the piezoresponse of the patterns [27 - 30]. Complex domain structure consisting of multiple domain patterns was found for ceramics studied (Figure 7, top row). To study the effect of the electric field on domain structure, a two square areas of 15 μm × 15 μm and 7.5 μm × 7.5 μm (structure "box-in-box") was scanned under a DC voltage of – 30 V and +30 V applying to the cantilever, respectively (Figure 7, middle row). Nucleation of single domains occurs under a sharp tip during the PFM testing reflecting development of domains and indicating ferroelectric polarization switching on nanoscale. The created domains are stable in the time. After 2 hours after the poling process, the PFM contrast of the written domains is the same (Figure 7, bottom row). Finally, remnant loops have been received on the samples using switching spectroscopy PFM (SS-PFM). Figure 6 shows the remnant d_{33}-V_{DC} piezoelectric hysteresis loops of the KNN-based ceramics calculated respectively from remnant PFM amplitude butterfly and PFM phase loops.

The highest effective d_{33} piezoelectric coefficient values reached 300 pm/V at V_{DC}=30 V in the samples with x=0.08 and 0.10 (Figure 8). Enhancement of the piezoelectric d_{33} value correlate well with formation of MPB with coexistence of orthorhombic and tetragonal phases observed (Figures 3), concentration dependences of spontaneous polarization (Figure 5*b*) and dielectric permittivity values measured at the room temperature (Figure 6).

Conclusions

Structure parameters, microstructure, dielectric, ferroelectric and piezoelectric properties of the $(1-x)(K_{0.5}Na_{0.5})NbO_3 - xLiSbO_3$ (x=0 - 0.1) ceramics were studied. Slight changes in the unit cell volume and temperatures of phase transitions were observed depending on composition and sintering

conditions. High values of the effective d_{33} piezoelectric coefficients ~ 300 pm/V were observed for ceramics with x=0.08 and x=0.1 confirming their prospects for development of new efficient piezoelectric materials.

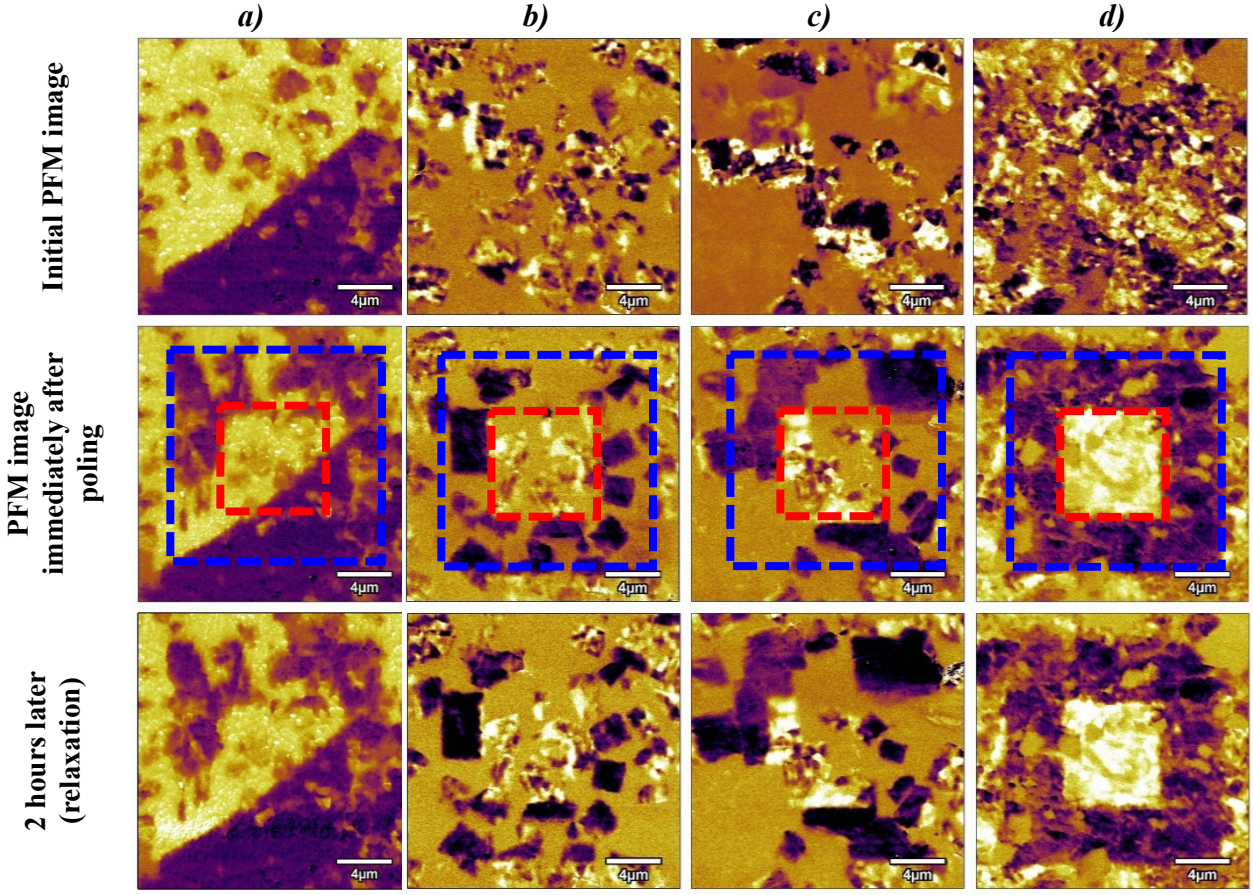

Figure 7 - Initial domain structure and temporary changes of images of polarized ceramics with x=0 (*a*), 0.06 (*b*), 0.08 (*c*), 0.10 (*d*).

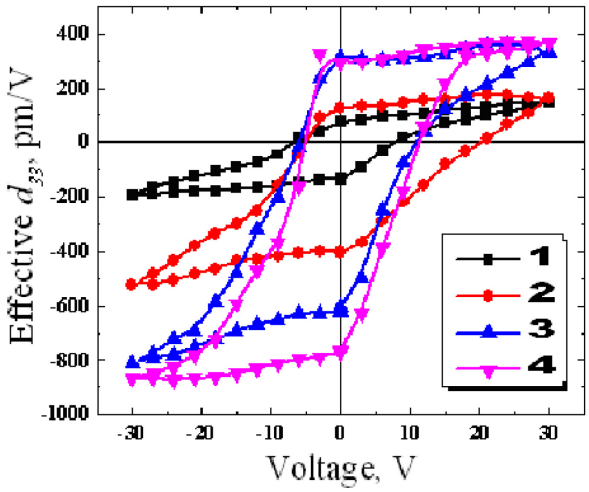

Figure 8 - Effective d_{33} values of the samples with x=0 (1), 0.06 (2), 0.08 (3) and 0.10 (4) calculated from PFM hysteresis loops for locations with large domain contrast.

Acknowledgment

The work was supported by the Russian Foundation for Basic Research (Project 18-03-00372).). PFM studies were performed at Center for Shared Use "Material Science and Metallurgy" at the National University of Science and Technology "MISiS" and were supported by the Ministry of Science and Higher Education of the Russian Federation (11.9706.2017/7.8).

References

[1]. S.J. Zhang, R. Xia, and R.T. Shrout, Lead-Free Piezoelectric Ceramics: Alternatives for PZT? J. Electroceram. 19 (2007) 251-257.

[2]. T. Takenaka, H. Nagata, and Y. Hiruma, Current developments and prospective of lead-free piezoelectric ceramics, Jpn. J. Appl. Phys. 47 (2008) 3787-3801.

[3]. P. K. Panda, Review: environmental friendly lead-free piezoelectric materials, J. Mater. Sci. 44 (2009) 5049-5062.

[4]. D. Damjanovich, N. Klein, J. Li and V. Porokhonskyy, What can be expected from lead-free piezoelectric materials?, Funct. Mater. Lett. 3 (2010) 5-13.

[5]. D.Q. Xiao, Progresses and further considerations on the research of perovskite lead-free piezoelectric ceramics, J. Adv. Dielectr. 1 (2011) 33-40.

[6]. Y.Q. Lu and Y.X. Li, A Review on Lead-Free Piezoelectric Ceramics Studies in China, J. Adv. Dielectr. 1 (2011) 269-288.

[7]. I. Coondoo, N. Panwar, A. Kholkin, Lead-free piezoelectrics: Current status and perspectives, J. Adv. Dielectr. 3 (2013) 1330002 (22 pages).

[8]. J.-F. Li, K. Wang, F.-Y. Zhu, L.-Q. Cheng, F.-Z. Yao, (K, Na)NbO_3-Based Lead-Free Piezoceramics: Fundamental Aspects, Processing Technologies, and Remaining Challenges, J. Am. Ceram. Soc. 96 (2013) 3677-3696.

[9]. J.G. Wu, D.Q. Xiao, J.G. Zhu, Potassium-sodium niobate lead-free piezoelectric materials: Past, present, and future of phase boundaries, Chem. Rev. 115 (2015) 2559-2595.

[10]. P.K. Panda and B. Sahoo, PZT to Lead-Free Piezo Ceramics, Ferroelectrics 474 (2015) 128-143.

[11]. C.H. Hong, H.P. Kim, B.Y. Choi, H.S. Han, J.S. Son, C.W. Ahn, W. Jo, Lead-free piezoceramics. Where to move on? J. Materiomics 2 (2016) 1-24.

[12]. Y.-J. Dai, X.-W. Zhang, and Ke-Pi Chen, Morphotropic phase boundary and electrical properties of $K_{1-x}Na_xNbO_3$ lead-free ceramics, Appl. Phys. Lett. 94 (2009) 042905.

[13]. H.-Y. Park, C.-W. Ahn, H.-C. Song, J.-H. Lee, and S. Nahma, Microstructure and piezoelectric properties of $0.95(Na_{0.5}K_{0.5})NbO_3$–$0.05BaTiO_3$ ceramics, App. Phys. Lett. 89 (2006) 062906.

[14]. J. Fang, X. Wang, R. Zuo, Z. Tian, C. Zhong, L. Li, Narrow sintering temperature window for (K,Na)NbO_3-based lead-free piezoceramics caused by compositional segregation, Phys. Status Solidi A. 208 (2011) 791-794.

[15]. K. Wang, J.-F. Li, J. (K,Na)NbO_3-based lead-free piezoceramics: Phase transition, sintering and property enhancement, Adv. Ceramics 1 (2012) 24-37.

[16]. R. Zuo, J. Roedel, R. Chen, L. Li, Sintering and electrical properties of lead-free $Na_{0.5}K_{0.5}NbO_3$ piezoelectric ceramics, J. Am. Ceram. Soc. 89 (2006) 2010-2015.

[17]. S. Zhang, R. Xia, T.R. Shrout, Modified $(K_{0.5}Na_{0.5})NbO_3$ based lead-free piezoelectrics with broad temperature usage range, Appl. Phys. Lett. 91 (2007) 132913.

[18]. J. Tellier, B. Malič, B. Dkhil, D. Jenko, J. Cilensek, M. Kosec, Crystal structure and phase transitions of sodium potassium niobate perovskites, Solid State Sci. 11 (2009) 320-324.

[19]. B. Malič, J. Koruza, J. Hreščak, J. Bernard, K. Wang, J.G. Fisher, A. Benčan, Sintering of lead-free piezoelectric sodium potassium niobate ceramics, Materials 12, (2015) 8117-8146.

[20]. E.D. Politova, G.M. Kaleva, N.V. Golubko, A.V. Mosunov, V.S. Akinfiev, S.Yu. Stefanovich, E.A. Fortalnova, Influence of NaCl/LiF Additives on Structure, Microstructure and Phase Transitions of $(K_{0.5}Na_{0.5})NbO_3$ Ceramics, Ferroelectrics 489 (2015) 147-155.

[21]. E.D. Politova, N.V. Golubko, G.M. Kaleva, A.V. Mosunov, N.V. Sadovskaya, S. Yu. Stefanovich, D.A. Kiselev, A.M. Kislyuk, P.K. Panda, Processing and characterization of lead-free ceramics on the base of sodium-potassium niobate, J. Adv. Diel. 8 (2018) 1850004.

[22]. M. E. Ringgaard and T.Wurlitzer, Lead-free piezoceramics based structure, microstructure and electrical properties of on alkali niobates, J. Eur . Ceram. Soc. 25 (2005) 2701-2706.

[23]. E.D. Politova, D.A. Strebkov, D.A. Belkova, , G.M. Kaleva, N.V. Golubko, V. Mosunov, N.V. Sadovskaya, P.K. Panda, Relaxation Effects in Nonstoichiometric NBT-Based Ceramics, Defect and Diffusion Forum, 391 (2019) 95-100.

[24]. E. D. Politova, N. V. Golubko, A. V. Mosunov, N. V. Sadovskaya, G. M. Kaleva, D. A. Kiselev & A. M. Kislyuk, Influence of additives on structure and ferroelectric properties of NBT-BT-BMT ceramics, Ferroelectrics, 531 (2018) 22-30.

[25]. V.V. Zhurov, S.A.Ivanov, PROFIT a program for powder diffraction data evaluation for IBM PC with a graphical user interface. Crystallography Reports, 42 (1997) 239-243.

[26]. Dunmin Lin, K. W. Kwok, K. H. Lam, and H. L. W. Chan. Structure and electrical properties of $K_{0.5}Na_{0.5}NbO_3$ –$LiSbO_3$ lead-free piezoelectric ceramics. Journal of Applied Physics, 101 (2007) 074111.

[27]. V.V. Shvartsman, D.C. Lupascu, Lead-Free Relaxor Ferroelectrics, J. Amer. Ceram. Soc. 95 (2012) 1-26.

[28]. W. Kleemann, Random-field induced antiferromagnetic, ferroelectric and structural domain states, Int. J. Mod. Phys. B 7 (1993) 2469-2507.

[29]. S. Jesse, A.P. Baddorf, S.V. Kalinin, Switching spectroscopy piezoresponse force microscopy of ferroelectric materials, Appl. Phys. Lett. 88 (2006) 062908.

[30]. H. Trivedi, V.V. Shvartsman, D.C. Lupascu, M.S. Medeiros, R.C. Pullar, A.L. Kholkin, P. Zelenovskiy, A. Sosnovskikh, V.Y. Shur, Local manifestations of a static magnetoelectric effect in nanostructured $BaTiO_3$–$BaFe_{12}O_9$ composite multiferroics, Nanoscale 7 (2015) 4489-4496.